

Digital Reconstruction From Fourier Projection Data

A Thesis

Presented to
the Faculty of the Graduate School
University of Houston

In Partial Fulfillment
of the Requirements for the Degree
Master of Science

by

Mark S. Egan

July 1978

Digital Reconstruction From Fourier Projection Data

An Abstract of a Thesis
Presented to
the Faculty of the Graduate School
University of Houston

In Partial Fulfillment
of the Requirements for the Degree
Master of Science

by
Mark S. Egan
July 1978

ABSTRACT

Presented is the theoretical basis for reconstruction of 2-dimensional signals in the Fourier plane from projection data. Three algorithms are studied in detail: the Hankel transform method, the 2-dimensional interpolation method, and the concentric squares raster method. Each algorithm is programmed and applied to simulated projection data. The results are compared.

The applicability of these techniques to mapping ultrasonic fields is considered, and the use of mini-computers discussed.

TABLE OF CONTENTS

	PAGE
I. Introduction	1
1.1 Opening Remarks	1
1.2 Theoretical Background	4
1.2.1 The Continuous Fourier Transform (CFT)	4
1.2.2 The Discrete Fourier Transform (DFT)	5
1.2.3 Projections and the Projection-Slice Theorem	6
1.3 An Overview	14
II. The Hankel Transform Method	18
2.1 Theory	18
2.2 Application and Results	23
2.3 Discussion	28
III. 2-Dimensional Linear Interpolation from Polar to Square Raster in the Fourier Domain	29
3.1 Theory	29
3.2 Application and Results	32
3.3 Discussion	36
IV. Concentric Squares Raster	38
4.1 Theory	38
4.2 Application and Results	41
4.3 Discussion	45

V.	A Final Word	46
	5.1 Conclusions	46
	5.1.1 Comparison	46
	5.1.2 Judgement	48
	5.2 Suggestions	49
	Bibliography	50
	Appendix	52

CHAPTER I

INTRODUCTION

1.1 Opening Remarks

There are many instances in life when it is desired to map some n -dimensional object. Often a direct mapping is impractical so indirect approaches must be taken. One such approach is the use of $n-1$ dimensional images. If a number of these images, or projections as we shall call them, can be obtained, then a reasonable estimate of the original signal can be derived.

The mathematician J. Radon (1) established the theoretical foundation for this, but the first practical use came in 1956 when Bracewell (2) searched for those areas of the sun which emit microwave radiation. By pointing his radio-telescope in several directions, Bracewell was able to obtain sufficient data to map the sun.

One of the best known applications in current technology is in the field of medicine. Computer-Aided-Tomography is used to reconstruct slices of the human brain. The input data are X-ray photographs called CAT-Scans, each taken at a different angle. A good introduction to this subject is given by Scudder (3).

Sound fields can be reconstructed from their projections. Such projections are recorded by using light beams. A specific case is the mapping of a transducer field

as discussed by Cook and Berlinghieri (4). As a matter of fact, this case is of particular interest since it is necessary to acquire data from but one projection to calculate the total field. This can be done by using elementary scalar wave theory as described by Cook (5). (See figure 1).

As one might expect, many other reconstruction examples exist in the medical and physical sciences. Applications in fields ranging from nuclear medicine to geophysics are surveyed in reference (6).

But just how can signals be recovered from projection data? Actually several avenues exist, but this paper shall concern itself with only one - digital reconstruction in Fourier space. Furthermore this study will tailor itself to the mapping of ultrasonic fields from acousto-optical data and the plausibility of doing so with mini-computers.

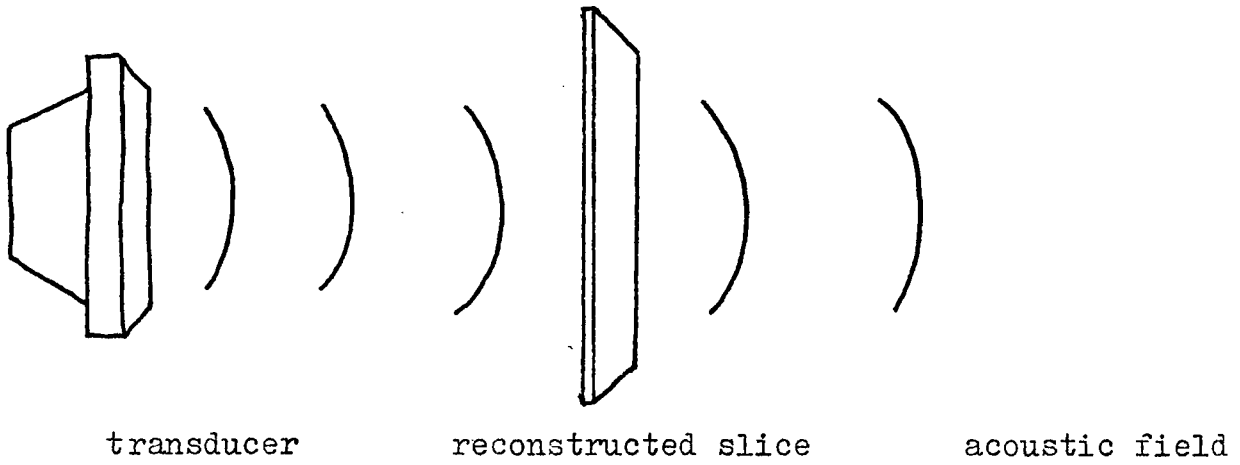


Figure 1 Reconstruction of an acoustic field

1.2 Theoretical Background

For this present work, we will be interested only in signals of 2 dimensions. The theory in general, however, can be extended to any finite dimension.

1.2.1 The Continuous Fourier Transform (CFT)

The definition of the 2-dimensional Fourier transform and its inverse is given by

$$F(\vec{w}) = \int_{\text{SIGNAL SPACE}} f(\vec{x}) e^{-j(\vec{w} \cdot \vec{x})} d\vec{x} \quad (1)$$

and

$$f(\vec{x}) = \frac{1}{4\pi^2} \int_{\text{FOURIER SPACE}} F(\vec{w}) e^{j(\vec{w} \cdot \vec{x})} d\vec{w} \quad (2)$$

where $\vec{x} = (x_1, x_2)$ is the vector in signal space, $\vec{w} = (w_1, w_2)$ the vector in Fourier space, and $\vec{w} \cdot \vec{x}$ the dot product of the two. These equations can of course be expanded into the more familiar forms

$$F(w_1, w_2) = \int_{-\infty}^{\infty} \int_{-\infty}^{\infty} f(x_1, x_2) e^{-j(w_1 x_1 + w_2 x_2)} dx_1 dx_2 \quad (1a)$$

and

$$f(x_1, x_2) = \int_{-\infty}^{\infty} \int_{-\infty}^{\infty} F(w_1, w_2) e^{j(w_1 x_1 + w_2 x_2)} dw_1 dw_2 \quad (2a)$$

We have assumed here that the variables x_1 and x_2 are continuous.

When x_1 and x_2 are discrete, the Fourier transform takes a different form as we shall next see.

1.2.2 The Discrete Fourier Transform (DFT)

Since we will be using the digital computer, all continuous functions will have to be digitized. This restricts us to using only band-limited functions.

The function $f(x_1, x_2)$ is said to be band-limited if there exists a 2-tuple (s_1, s_2) such that $F(w_1, w_2)$ is zero whenever $|w_1| > 2\pi s_1$ or $|w_2| > 2\pi s_2$.

When we sample $f(x_1, x_2)$ we must be sure to have a sampling frequency f_i in each dimension x_i such that $f_i > 2s_i$. Since $w_i = 2\pi f_i$, this is equivalent to saying $w_i > 4\pi s_i$. This will result in a rectangular lattice of data points; and by the n-Dimensional Sampling Theorem, the continuous function $f(x_1, x_2)$ will be completely recoverable from this lattice.

The DFT is a transform in its own right, with many of its properties analogous to those of the CFT. The exact form of the DFT is most easily understood in 1-dimension:

$$w_k = \frac{1}{2\pi} \sum_{n=0}^{N-1} t_n e^{-j\frac{2\pi kn}{N}} \quad k = 0, 1, \dots, (N-1)$$

(3)

where w_k is the k^{th} frequency sample and t_n the n^{th} signal sample. For dimensions higher than the first, the

equation becomes considerably more complicated. There is no need to elaborate further here, but the interested reader is referred to Mersereau and Oppenheim (8).

There are several ways to program the DFT, but none surpass the fast Fourier transform algorithms in terms of speed and economy. These FFT techniques have understandably received much attention in recent literature. See references (9), (10), and (11).

1.2.3 Projections and the Projection-Slice Theorem

The input to the reconstruction routines considered in this study is a special class of images. An understanding of how these images relate to the original signal is central in the development of these routines.

To this end, let $f(x_1, x_2)$ define some 2-dimensional object. (See figure 2). By integrating f along lines which are parallel to the x_2 axis, we obtain a 1-dimensional function denoted by p . (See figure 3).

$$p_{x_2}(x_1) = \int_{-\infty}^{\infty} f(x_1, x_2) dx_2 \quad (4)$$

If we take the 1-dimensional Fourier transform of p , we get:

$$\begin{aligned} P_{x_2}(w_1) &= \int_{x_1=-\infty}^{\infty} \int_{x_2=-\infty}^{\infty} f(x_1, x_2) e^{-j(w_1 x_1)} dx_2 dx_1 \\ &= \int_{x_1=-\infty}^{\infty} \int_{x_2=-\infty}^{\infty} f(x_1, x_2) e^{-j(w_1 x_1 + w_2 x_2)} dx_2 dx_1 \end{aligned}$$

where $w_2 = 0$

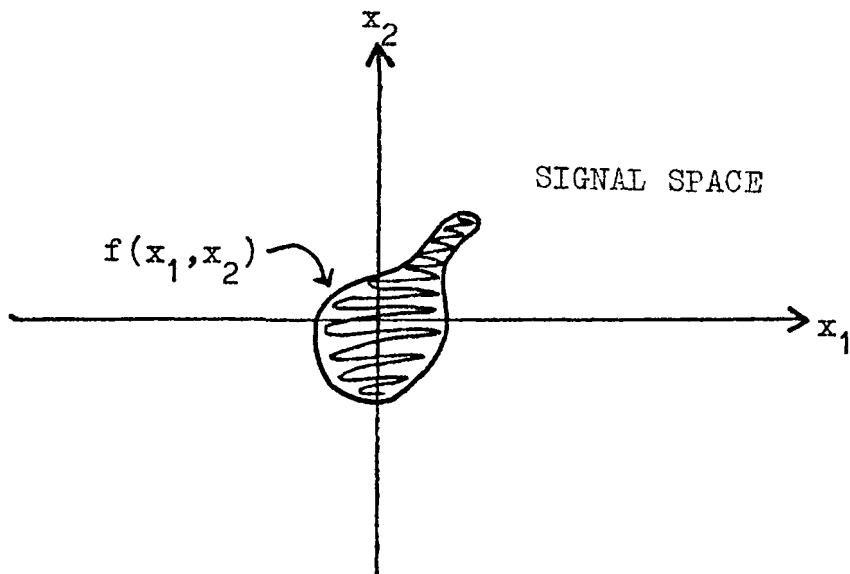


Figure 2 Signal to be reconstructed

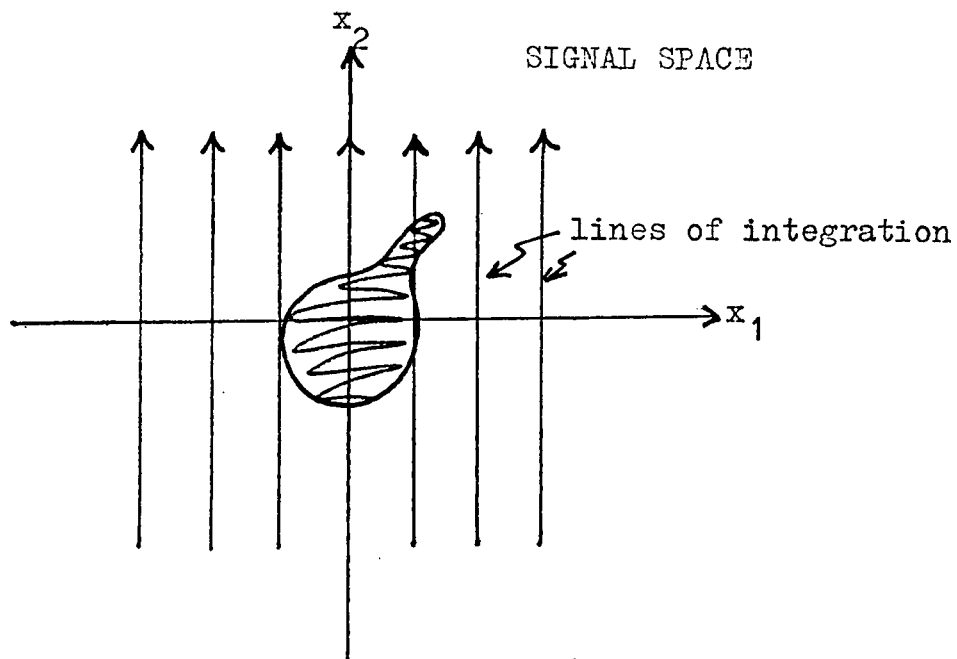


Figure 3 Lines of integration for obtaining a projection

$$= F(w_1, w_2) \Big|_{w_2 = 0} \quad 8 \quad (5)$$

where $F(w_1, w_2)$ is the 2-dimensional Fourier transform of f . That is, the 1-dimensional Fourier transform of p is the slice in the Fourier plane, F , evaluated along the line $w_2 = 0$. This is displayed in figure (4).

Now let us integrate f in some other direction. Let the lines of integration be those which are perpendicular to the x_1' axis as shown in figure (5). To perform this integration, we merely have to rotate the coordinate axes (back) by the angle $-\theta$, and then integrate as before.

Recall that

$$\begin{aligned} x_1' &= x_1 \cos \theta + x_2 \sin \theta \\ x_2' &= -x_1 \sin \theta + x_2 \cos \theta \end{aligned} \quad (6)$$

In matrix form this is

$$\begin{pmatrix} x_1' \\ x_2' \end{pmatrix} = \begin{pmatrix} \cos \theta & \sin \theta \\ -\sin \theta & \cos \theta \end{pmatrix} \begin{pmatrix} x_1 \\ x_2 \end{pmatrix}, \quad (6a)$$

or more succinctly

$$\vec{x}' = A \vec{x} \quad (6b)$$

where A is the rotation matrix in the $+\theta$ direction.

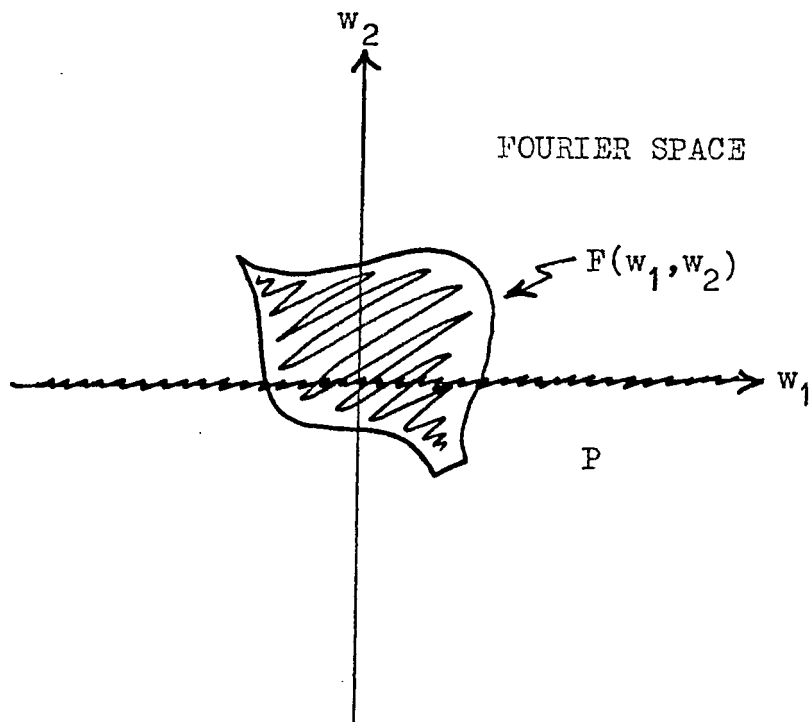


Figure 4 Slice in Fourier domain obtained by transforming a projection

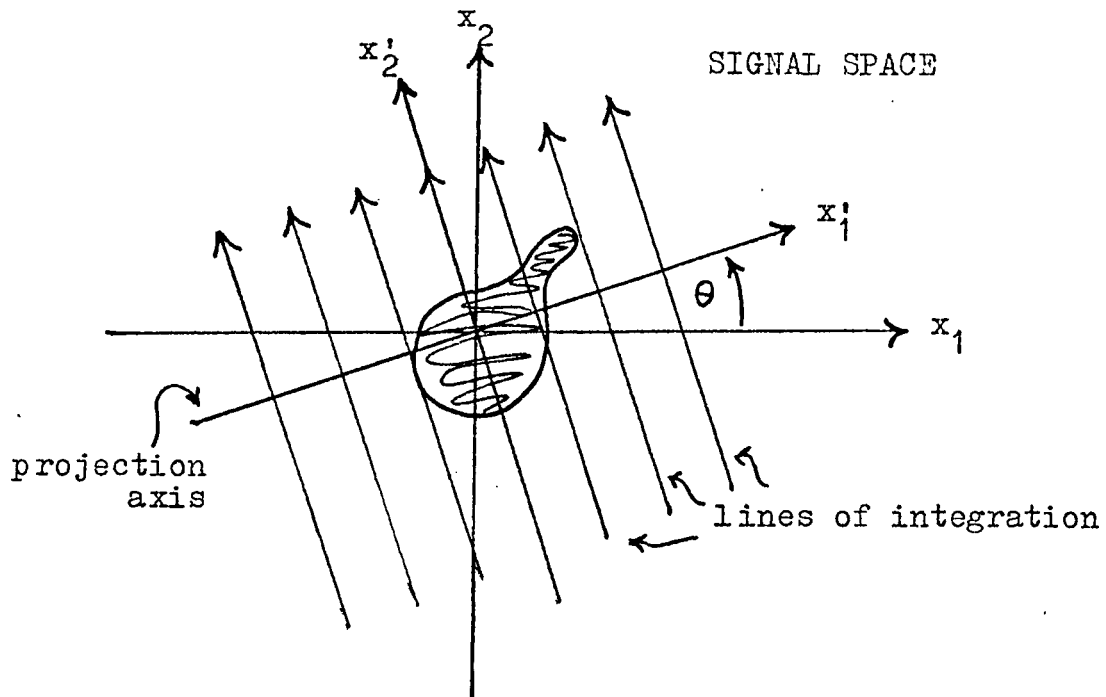


Figure 5 Lines of integration for obtaining another projection

Thus

$$\begin{aligned}
 p_{\theta}(x_1') &\equiv p_{x_2'}(x_1') \\
 &= \int_{-\infty}^{\infty} f(\vec{x}) dx_2' & (7) \\
 &= \int_{-\infty}^{\infty} f(A^{-1}\vec{x}') dx_2' & (7a) \\
 &= \int_{-\infty}^{\infty} f(x_1' \cos \theta - x_2' \sin \theta, x_1' \sin \theta + x_2' \cos \theta) dx_2'. & (7b)
 \end{aligned}$$

Equation (7b) is the general definition of a projection in 2 dimensions. We see that p_{θ} is the 1-dimensional image of the 2-dimensional function f , obtained by integrating f along lines which are perpendicular to an axis which is moved an angle θ from the horizontal. This axis is called the projection axis.

We note that equation (4) describes a projection of f obtained with $\theta = 0$.

As before let us take the 1-dimensional Fourier transform of p_{θ} :

$$P(w_1') = \int_{-\infty}^{\infty} p_{\theta}(\vec{x}_1') e^{-j(w_1' x_1')} dx_1' \quad (8)$$

$$= \int_{-\infty}^{\infty} \int_{-\infty}^{\infty} f(\vec{x}) e^{-j(w_1' x_1')} dx_2' dx_1' \quad (9)$$

$$= \int_{-\infty}^{\infty} \int_{-\infty}^{\infty} f(\vec{x}) e^{-j(w_1' x_1' + w_2' x_2')} dx_2' dx_1'$$

where $w_2' = 0$

$$(10)$$

$$= \int_{-\infty}^{\infty} \int_{-\infty}^{\infty} f(\vec{x}) e^{-j(\vec{w}' \cdot \vec{x}')} dx_2' dx_1' \quad \text{where } w_2' = 0 \quad (11)$$

There is a useful theorem which states that if $f(\vec{x})$ and $F(\vec{w})$ are a Fourier transform pair, and if Q is an orthogonal transformation, then $f(Q\vec{x})$ and $F(Q\vec{w})$ also form a Fourier transform pair. Thus by rotating the vector \vec{x} through the angle θ to get \vec{x}' , we are also rotating the vector \vec{w} through θ to get \vec{w}' . This coupled with the fact that dot products are invariant to rotations implies that $\vec{w} \cdot \vec{x} = \vec{w}' \cdot \vec{x}'$. Now since $dx_1 dx_2 = dx_1' dx_2'$, with the Jacobian $\begin{vmatrix} \cos \theta & \sin \theta \\ -\sin \theta & \cos \theta \end{vmatrix}$ being equal to 1, we can rewrite equation (11) to obtain

$$P_{\theta}(w_1') = \int_{-\infty}^{\infty} \int_{-\infty}^{\infty} f(\vec{x}) e^{-j(\vec{w}' \cdot \vec{x}')} dx_2' dx_1' \quad \text{where } w_2' = 0 \quad (12)$$

Equation (12), of course, is just the 2-dimensional Fourier transform of $f(\vec{x})$ evaluated along the line $w_2' = 0$:

$$P_{\theta}(w_1') = F(\vec{w}) \Big|_{w_2' = 0} \quad (12a)$$

Figure (6) illustrates this fact.

What this means is that by taking the projection of signal f at an angle θ , and then performing the 1-dimensional Fourier transform on it, we obtain a slice of the Fourier plane, F . Furthermore this slice is also

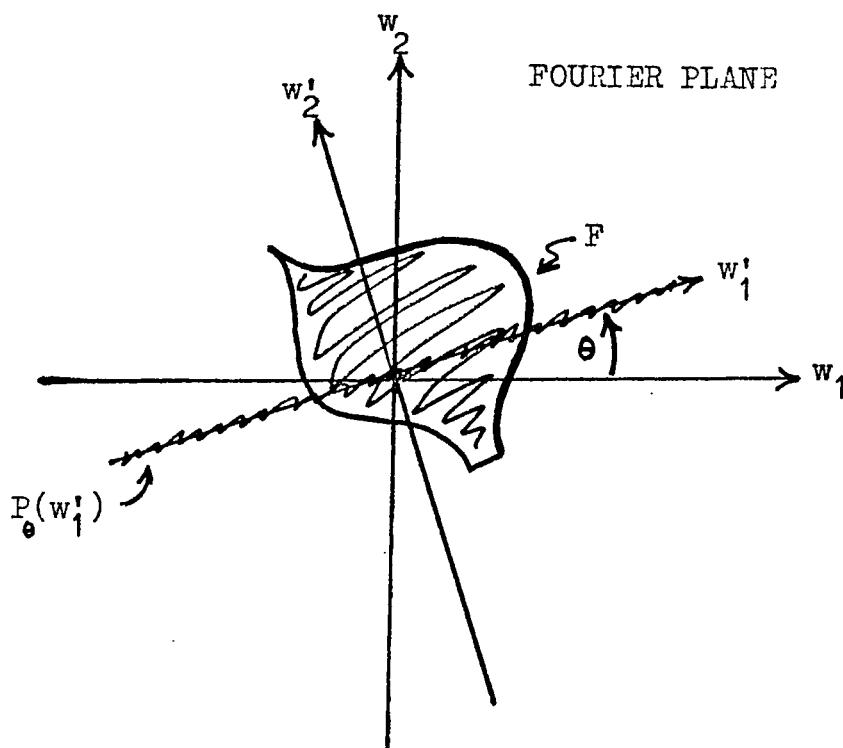


Figure 6 Slice of Fourier domain obtained from projection in figure (5)

oriented at the angle θ . This important fact is known as the Projection-Slice Theorem. The implications of this are that the complete Fourier plane can be determined by taking enough projections in the signal plane. Once this has been done, the original signal can be recovered. One obvious way of doing this would be to take the 2-dimensional inverse Fourier transform of F .

In most cases however, the Fourier plane cannot be specified in its entirety since only a finite number of projections can be obtained. Thus a number of digital algorithms have arisen. The next few chapters discuss the theory and application of three such techniques.

1.3 An Overview

The methods studied here all start in a similar fashion - transformation of projection data from signal to Fourier domain. By virtue of the Projection-Slice Theorem, the Fourier data points are arranged in a polar raster. (See figure 7).

Chapter II deals with a reconstruction technique which makes use of the data in this form. Chapters III and IV deal with methods which require the Fourier data be arranged in a Cartesian raster. Indeed the primary thrust of these schemes is conversion from the one raster to the other.

A word is in order now about the projection data. For each of the three applications, these data points are generated in a separate simulation program. Although any number of sample points can be output, only a modest number are actually produced. This reflects the capabilities of moderate acousto-optical apparatus that would be used to collect actual acoustic projection data. Furthermore it is desired to study the feasibility of programming these reconstruction algorithms on small computers. Thus the number of sample points is restrained by the size of computer memory.

Throughout the study therefore, 16 projection angles are used with 32 samples per projection. Extra data points of zero amplitude are added at the ends of each projection, bringing the total number of points per angle to 64. This is equivalent to desampling the data in reciprocal space, improving continuity. This padding of zeroes also

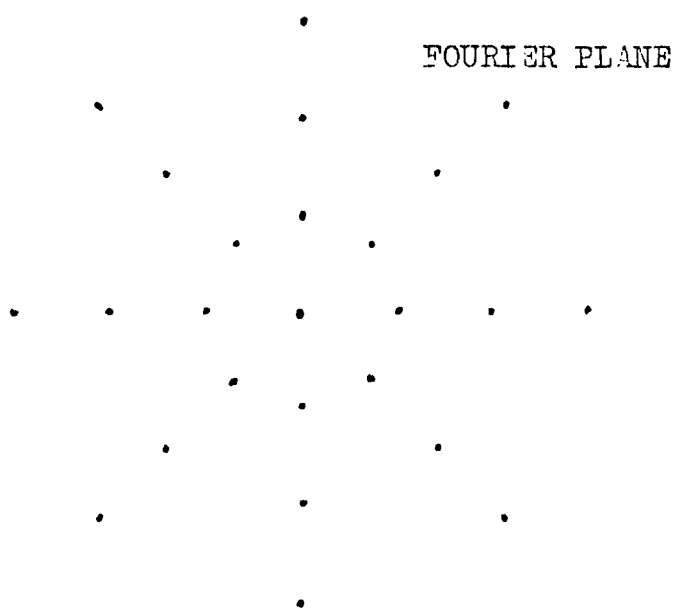


Figure 7 Polar raster

reduces problems caused by the cyclic nature of the DFT.

The specimen which is simulated in the following case studies is a square of unit density measuring 2 units to a side. A diagram of this specimen is shown in figure (8).

In the case of the Hankel Transform Method (Chapter II), a disk of unit density and unit radius is also modeled. This is portrayed in figure (9).

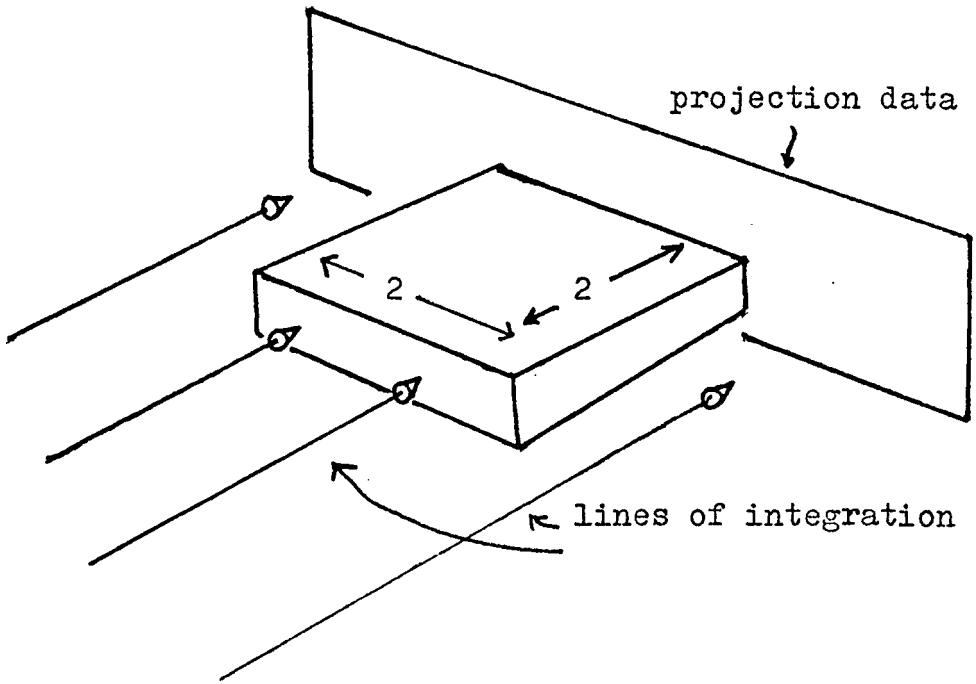


Figure 8 Square specimen of unit density

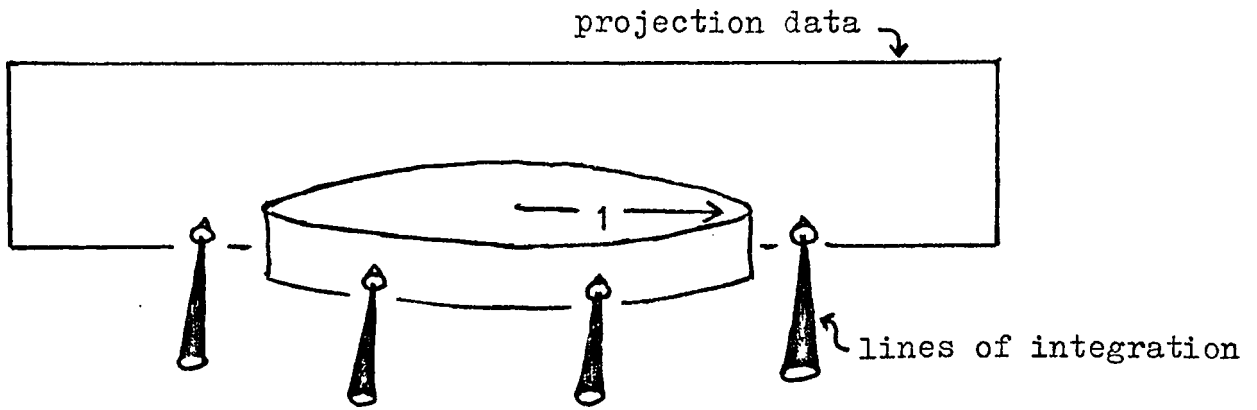


Figure 9 Circular specimen of unit density

CHAPTER II
THE HANKEL TRANSFORM METHOD

2.1 Theory

From the definition of the 2-dimensional CFT we have

$$F(\vec{w}) = \int_{\text{SIGNAL SPACE}} f(\vec{x}) e^{-j(\vec{w} \cdot \vec{x})} d\vec{x} \quad .$$

The definition of the dot product of two vectors implies that :

$$F(\vec{w}) = \int_{\text{SIGNAL SPACE}} f(\vec{x}) e^{-j|\vec{w}||\vec{x}| \cos \alpha} d\vec{x} \quad (13)$$

where α is the angle between vectors \vec{w} and \vec{x} . Figure (10) illustrates the relationships among ϕ , θ , and α . Since $\alpha = \theta - \phi$, we get:

$$F(\vec{w}) = \int_{\text{SIGNAL SPACE}} f(\vec{x}) e^{-j|\vec{w}||\vec{x}| \cos(\theta - \phi)} d\vec{x} \quad . \quad (14)$$

If polar coordinates are used, the Fourier transform pair appears like so:

$$F(\rho, \theta) = \int_{-\pi}^{\pi} \int_0^{\infty} f(r, \phi) e^{-j\rho r \cos(\theta - \phi)} r dr d\phi \quad (15)$$

and

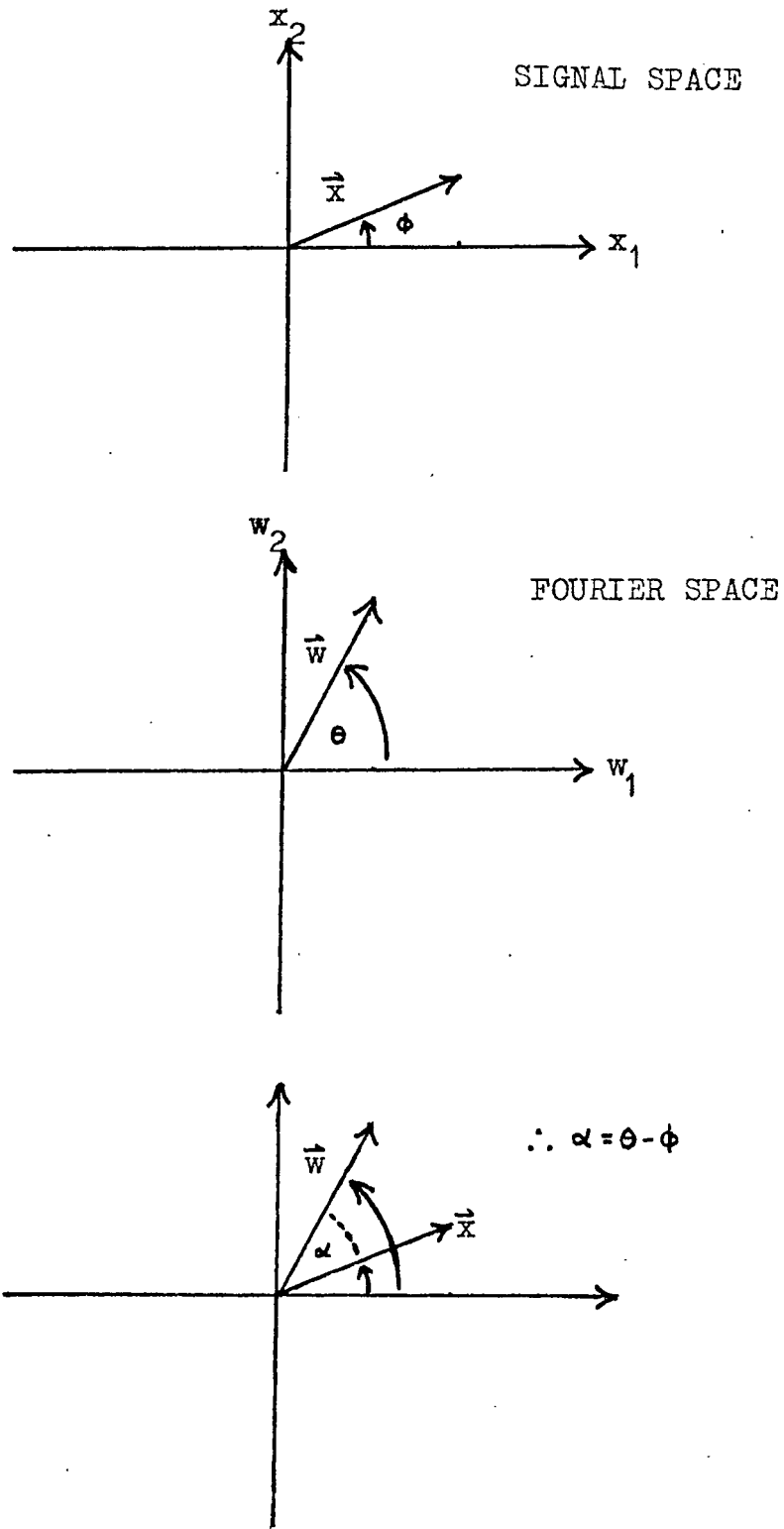


Figure 10 The directional relationship between vectors \vec{w} and \vec{x}

$$f(r, \phi) = \frac{1}{4\pi^2} \int_{-\pi}^{\pi} \int_0^{\infty} F(\rho, \theta) e^{j\rho r \cos(\theta - \phi)} \rho \, d\rho \, d\theta \quad (16)$$

where we have set $r = |\vec{x}|$ and $\rho = |\vec{w}|$.

Since $f(r, \phi)$ is necessarily a periodic function in ϕ with period 2π , it can be expressed in a Fourier series:

$$f(r, \phi) = \sum_{n=-\infty}^{\infty} f_n(r) e^{jn\phi} \quad (17)$$

where

$$f_n(r) = \frac{1}{2\pi} \int_{-\pi}^{\pi} f(r, \phi) e^{-jn\phi} d\phi \quad (18)$$

Substituting equation (16) into equation (18), we get:

$$f_n(r) = \frac{1}{2\pi} \int_{-\pi}^{\pi} \left[\frac{1}{4\pi^2} \int_{-\pi}^{\pi} \int_0^{\infty} F(\rho, \theta) e^{j\rho r \cos(\theta - \phi)} \rho \, d\rho \, d\theta \right] e^{-jn\phi} d\phi \quad (19)$$

$$= \frac{1}{8\pi^3} \int_{-\pi}^{\pi} \int_0^{\infty} F(\rho, \theta) \rho \left[\int_{-\pi}^{\pi} e^{j[\rho r \cos(\theta - \phi) - n\phi]} d\phi \right] d\rho \, d\theta \quad (20)$$

Using Appendix A this becomes

$$f_n(r) = \frac{1}{8\pi^3} \int_{-\pi}^{\pi} \int_0^{\infty} F(\rho, \theta) \rho \left[2\pi e^{-jn(\theta - \pi/2)} J_n(\rho r) \right] d\rho \, d\theta \quad (21)$$

which implies

$$f_n(r) = \frac{1}{2\pi} \int_0^{\infty} \left[\frac{1}{2\pi} \int_{-\pi}^{\pi} F(\rho, \theta) e^{-jn\theta} d\theta \right] e^{jn\pi/2} J_n(\rho r) \rho d\rho \quad (22)$$

But since $F(\rho, \theta)$ is periodic with period 2π , it too can be expressed in a Fourier series:

$$F(\rho, \theta) = \sum_{n=-\infty}^{\infty} F_n(\rho) e^{jn\theta} \quad (23)$$

where

$$F_n(\rho) = \frac{1}{2\pi} \int_{-\pi}^{\pi} F(\rho, \theta) e^{-jn\theta} d\theta \quad (24)$$

Substituting equation (24) into equation (22) yields

$$f_n(r) = \frac{1}{2\pi} \int_0^{\infty} F_n(\rho) e^{jn\pi/2} J_n(\rho r) \rho d\rho \quad (25)$$

or

$$f_n(r) = \frac{1}{2\pi} \int_0^{\infty} \hat{F}_n(\rho) J_n(\rho r) \rho d\rho \quad (26)$$

where

$$\hat{F}_n(\rho) \equiv F_n(\rho) e^{jn\pi/2} \quad (27)$$

By inspection we see that $f_n(r)$ and $\hat{F}_n(\rho)$ form a Hankel transform pair:

$$f_n(r) = \frac{1}{2\pi} \int_0^{\infty} \hat{F}_n(\rho) J_n(\rho r) \rho d\rho \quad (26)$$

and

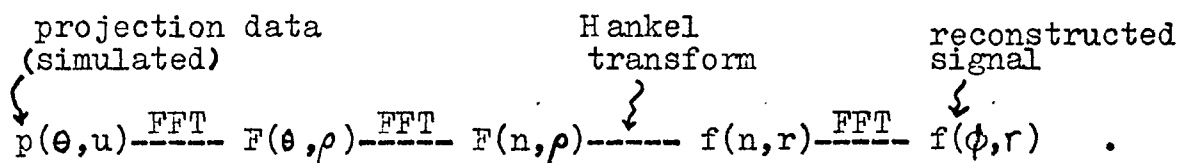
$$\hat{F}_n(\rho) = \int_0^{\infty} f_n(r) J_n(\rho r) r dr \quad . \quad (28)$$

We now have everything we need to outline a reconstruction algorithm.

1. Collect the projection data.
2. Take the Fourier transform of these projections to obtain $F(\rho, \theta)$.
3. Calculate $\hat{F}_n(\rho)$ from $F(\rho, \theta)$ by using equations (24) and (27).
4. Take the Hankel transform of $\hat{F}_n(\rho)$ to get $f_n(r)$.
5. Find $f(r, \phi)$, the reconstructed signal, by using equation (17).

2.2 Application and Results

The above algorithm, as applied in this study, can be represented schematically:



As can be seen, the FFT is used whenever possible. More specifics will be given later, but let us now look at some results.

The first case presented here is that of the disk. Fortunately, study shows that there is no need to apply an anti-alias filter to these projection data since there are no appreciable amplitudes above the Nyquist frequency. Thus reconstruction can begin from the raw input sample points.

By nature of the Hankel transform method, reconstructions represent diametric slices of the original signal. Since a disk has radial symmetry, all slices appear the same. An example slice is shown in figure (11).

The next specimen is the square. Again the data are already band-limited. Reconstructions for various angles are presented in figures (12), (13), and (14).

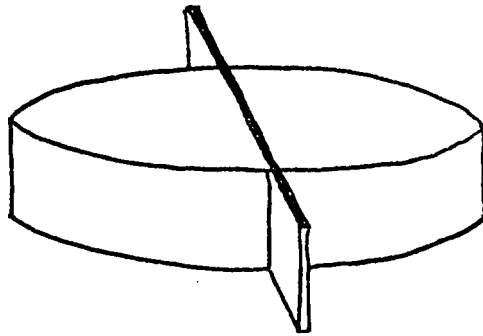


Figure 11a Orientation of output slice

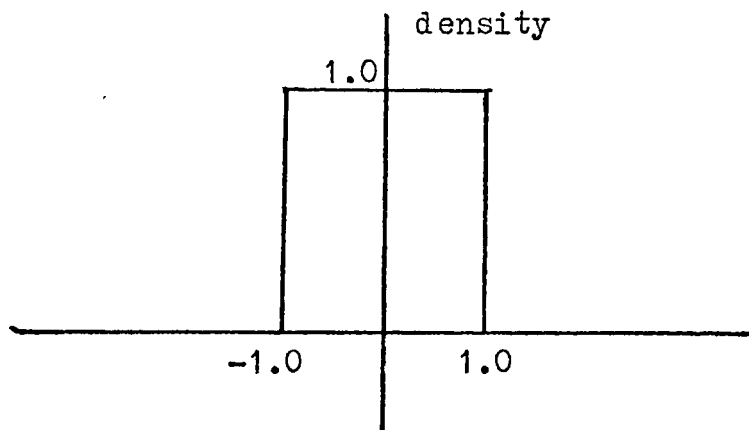


Figure 11b Ideal reconstruction



Figure 11c Actual reconstruction

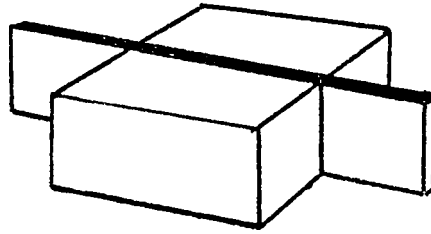


Figure 12a Orientation of output slice

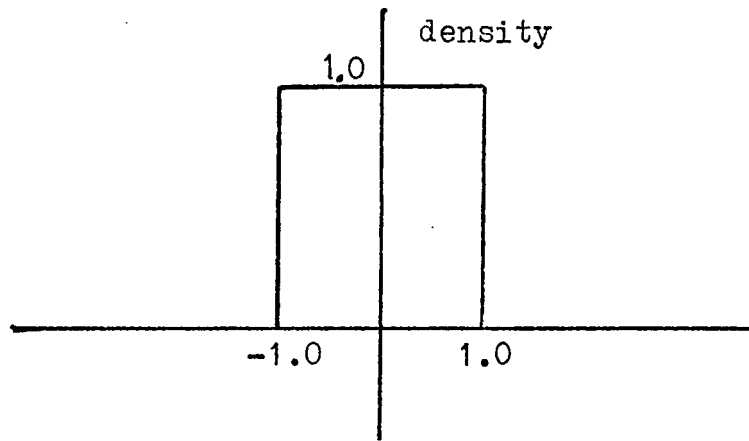


Figure 12b Ideal reconstruction



Figure 12c Actual reconstruction

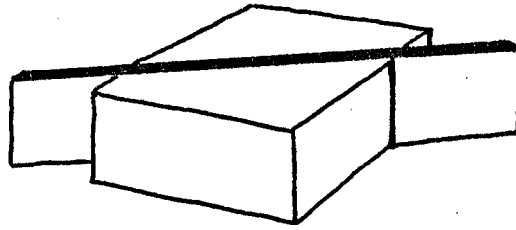


Figure 13a Orientation of output slice

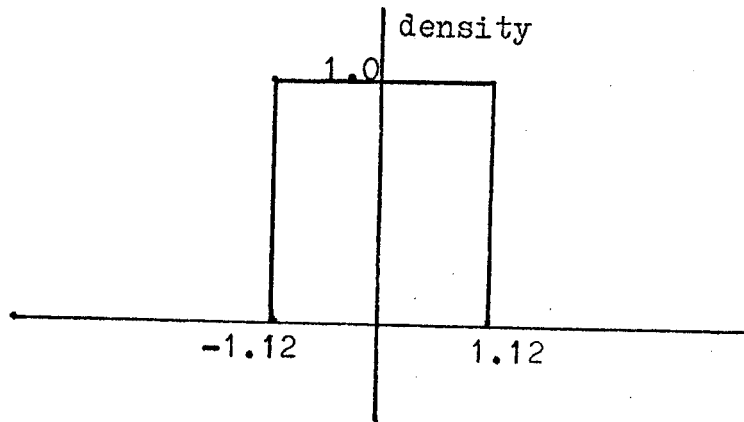


Figure 13b Ideal reconstruction

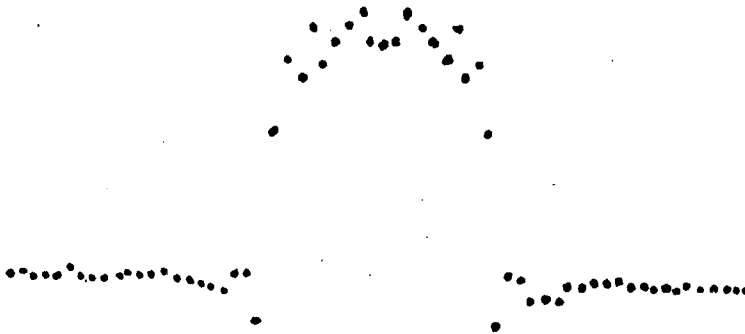


Figure 13c Actual reconstruction

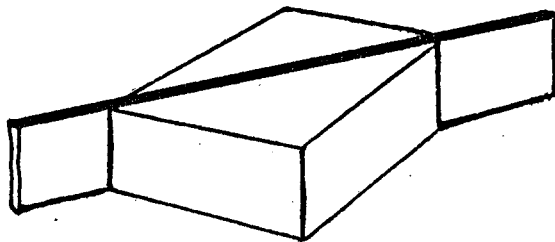


Figure 14a Orientation of output slice

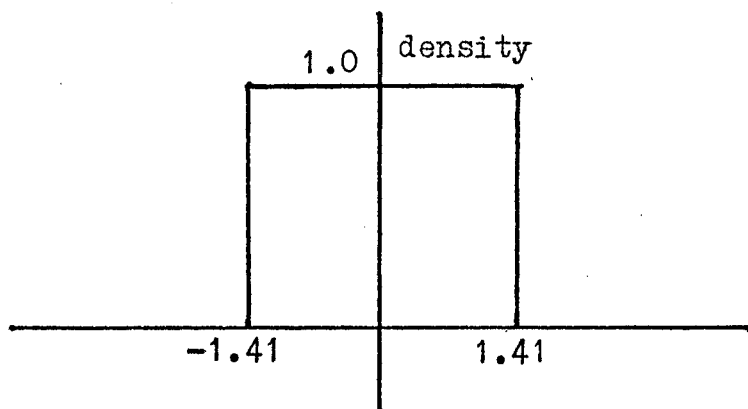


Figure 14b Ideal reconstruction

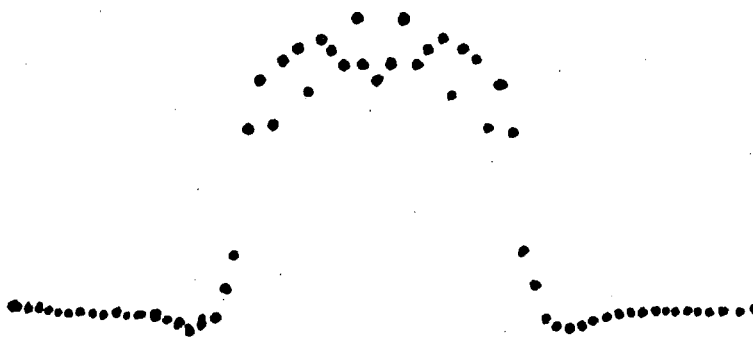


Figure 14c Actual reconstruction

2.3 Discussion

The Hankel transform method is convenient in that it makes ready use of the Fourier data in polar form. When programming this technique however, a number of serious drawbacks were observed.

Many Hankel transforms had to be taken, and each one required a different Bessel function. These functions varied widely in order and argument. Since no one algorithm could be found which would converge for each case, several methods had to be used. Exponent overflows and underflows were everpresent problems. In addition, excessive demands were made on CPU^U time. Eventually these problems were circumnavigated by generating a large table of Bessel functions in a separate program. This table was then input to the reconstruction program and functions were linearly interpolated as needed.

In calculating the Hankel integral itself, a routine was needed which would converge quickly. Enough terms were needed to keep truncation error at a minimum, yet too many terms would cause round-off error to explode. Neither the trapezoid rule nor Simpson's rule were adequate. It was found that Romberg integration performed reasonably well, but only if the optimum number of terms were used. A lucid development of Romberg integration is given in reference (12).

CHAPTER III

2-DIMENSIONAL LINEAR INTERPOLATION FROM POLAR
TO SQUARE RASTER IN THE FOURIER DOMAIN3.1 Theory

One would think that once the data in the Fourier plane is determined, the most straightforward way to reconstruct the signal would be to take the 2-dimensional inverse Fourier transform. Indeed the simplicity of this approach is appealing. However there is one obstacle that must first be overcome.

In order to use the 2-dimensional inverse FFT, the data must be arranged in a Cartesian or rectangular raster (figure 15). As mentioned before however, by virtue of the Projection-Slice Theorem, the sample points in the Fourier plane are oriented in a polar raster (figure 7).

Consequently before the inverse FFT can be taken, the data in the Fourier plane must be rearranged. Interpolation schemes abound, but the most familiar one of course is the technique of linear interpolation.

Using this method, we approximate the value at an interpolated point by the weighted average of the four surrounding data points. See figure (16). The formula for this interpolation is:

$$F(P_{int}) = \frac{\frac{1}{d_1}F(P_1) + \frac{1}{d_2}F(P_2) + \frac{1}{d_3}F(P_3) + \frac{1}{d_4}F(P_4)}{\frac{1}{d_1} + \frac{1}{d_2} + \frac{1}{d_3} + \frac{1}{d_4}} \quad (29)$$

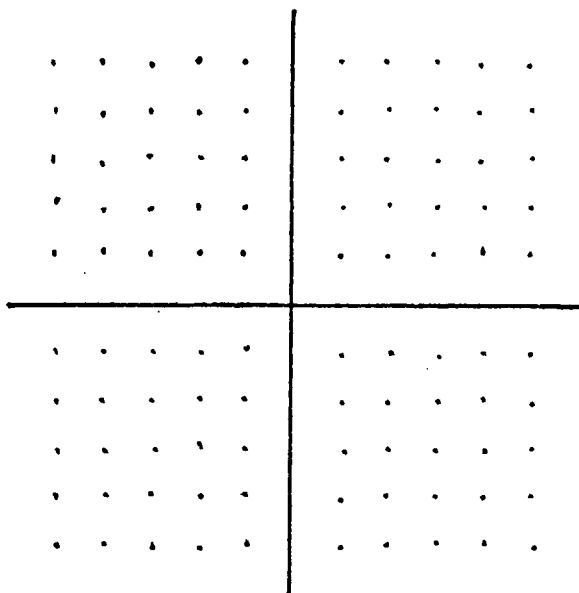


Figure 15 Cartesian raster

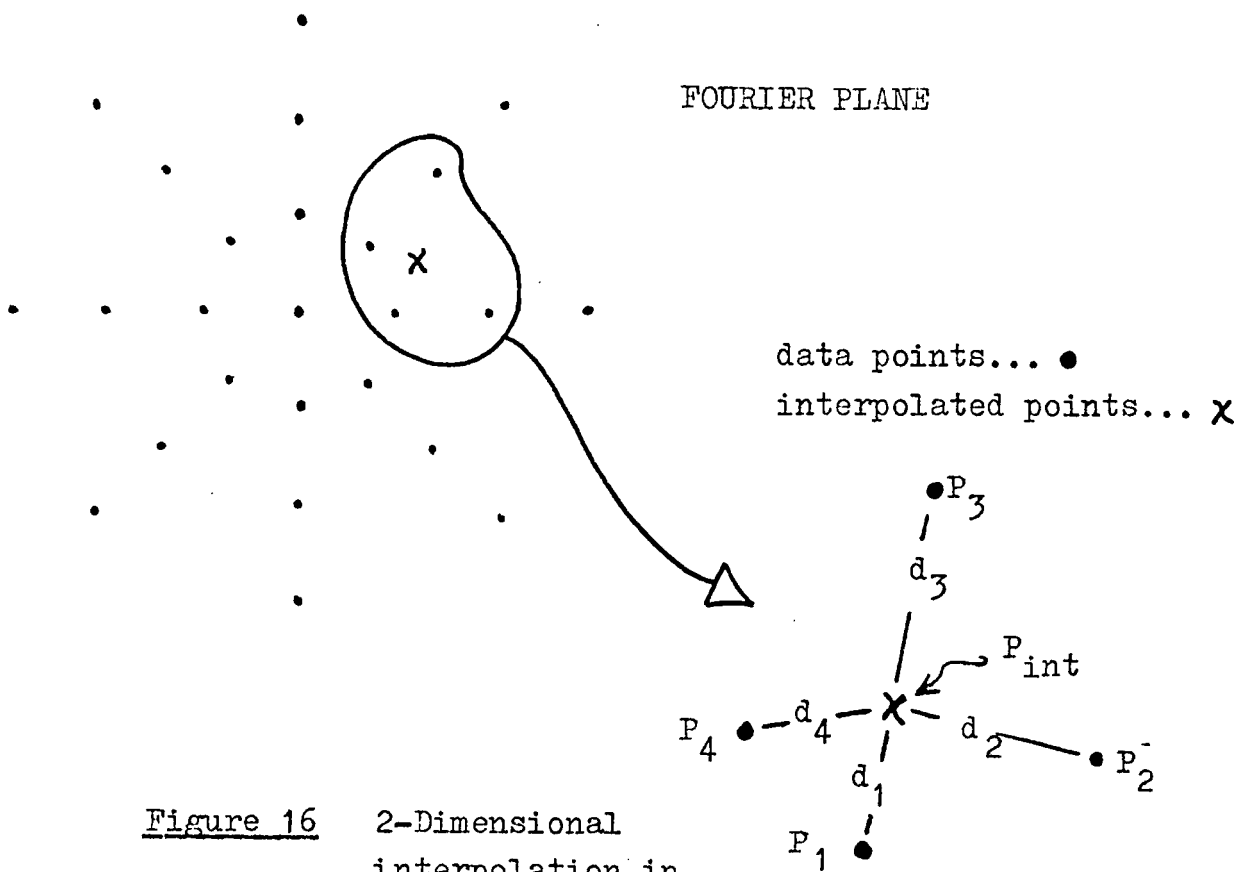


Figure 16 2-Dimensional interpolation in the Fourier plane

Thus we have the following reconstruction algorithm:

1. Collect the projection data.
2. Transform each projection to the Fourier plane to obtain a polar raster.
3. Linearly interpolate the points to a Cartesian raster.
4. Use the 2-dimensional inverse transform to go back to the signal domain.

3.2 Application and Results

The FFT is again used wherever possible for the sake of efficiency. With this technique, the reconstructed signal is specified in Cartesian form rather than polar form as in the case of the Hankel transform method.

The primary specimen here is a square of unit density. Some reconstructions are presented below.

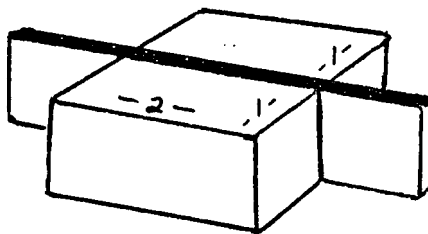


Figure 17a Orientation of output slice

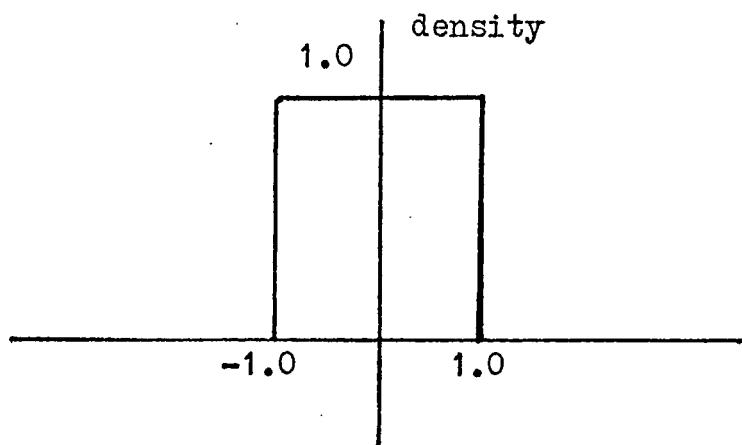


Figure 17b Ideal reconstruction



Figure 17c Actual reconstruction

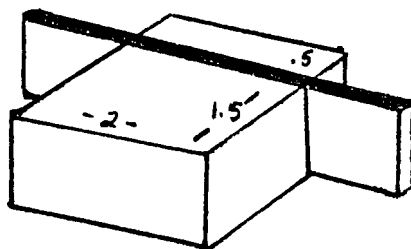


Figure 18a Orientation of output slice

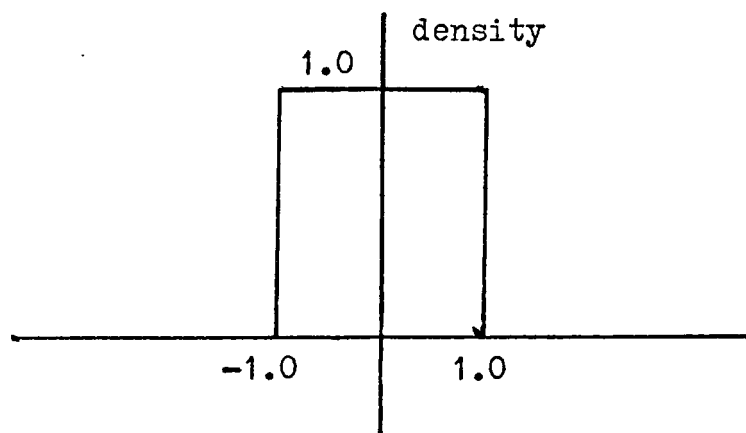


Figure 18b Ideal reconstruction



Figure 18c Actual reconstruction

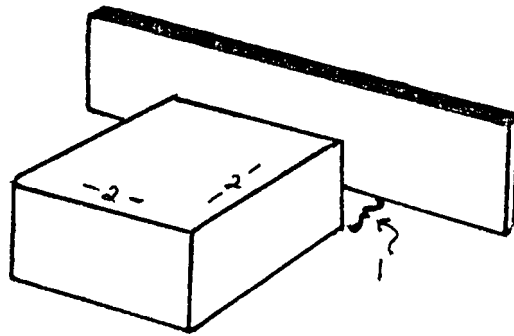


Figure 19a Orientation of output slice

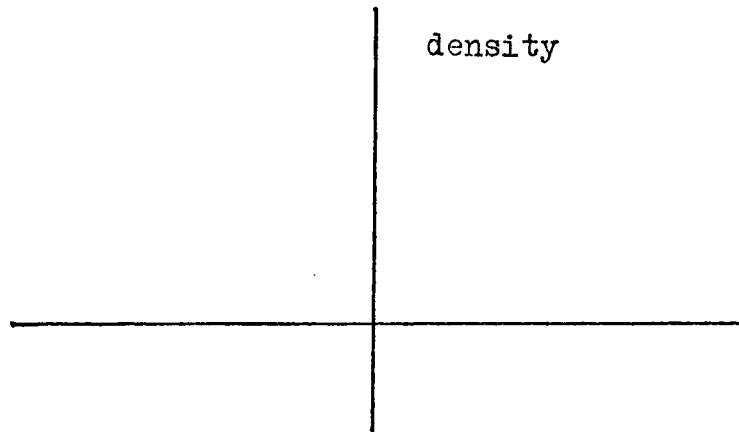


Figure 19b Ideal reconstruction

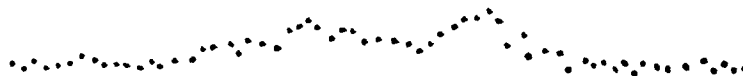


Figure 19c Actual reconstruction

3.3 Discussion

Since there are no lengthy calculations to be made, this technique runs quite quickly on the computer. Due to the interpolation approximations though, a certain amount of error is inherent in this method, especially on the perimeter of the Fourier plane. Near the origin, the data points are closely packed giving rise to accurate interpolations. Far from the origin however, the sparcity of the data points makes good approximations difficult. Figure (20) shows this graphically.

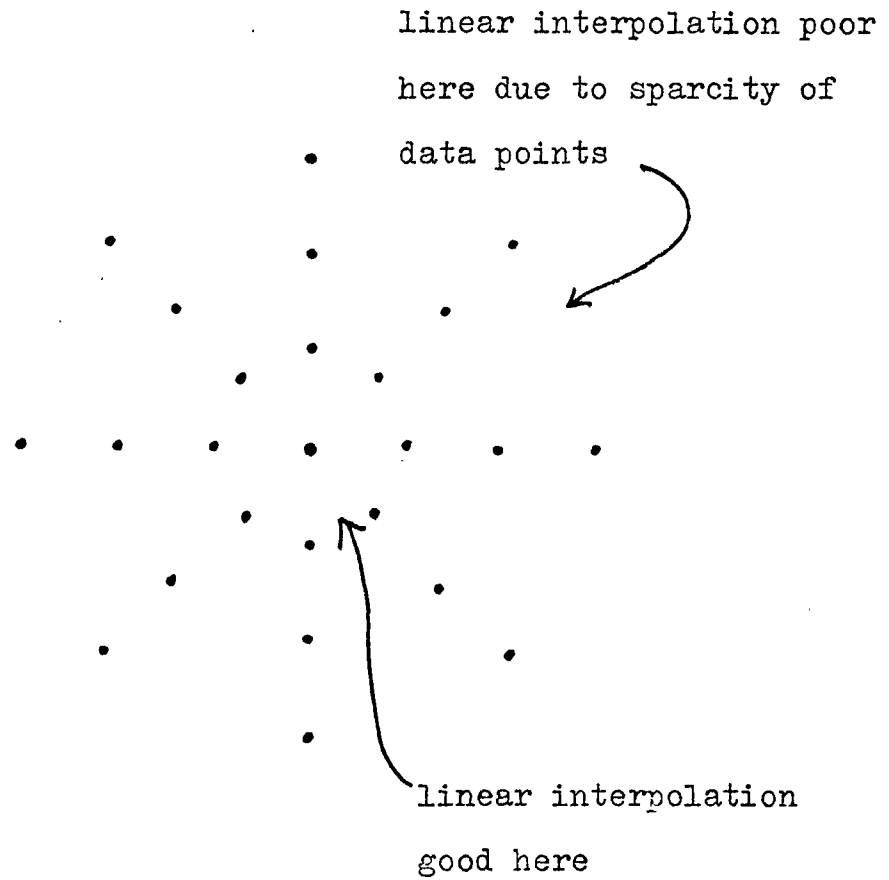


Figure 20 Interpolation from a polar raster

CHAPTER IV
CONCENTRIC SQUARES RASTER

4.1 Theory

It is possible to simplify the previous chapter's interpolation in the Fourier plane. If the input sampling frequency is varied according to the projection angle in some specific manner, one can produce an arrangement in the Fourier domain which approximates a Cartesian raster. This configuration is known as the concentric squares raster and is shown in figure (21).

By using only 1-dimensional interpolation, it is possible to fill in the missing points (figure 22). In figure (23), for instance, data points A and B are used for the interpolation of points C and D.

It would seem that 1-dimensional interpolation could have an advantage over 2-dimensional interpolation since fewer calculations would be necessary. Run time and round-off error would thus diminish.

Here then is the algorithm:

1. Collect the data, varying the sampling frequency such that
2. a concentric squares raster is formed after transformation to the Fourier domain.
3. Use 1-dimensional interpolation to complete the Cartesian raster.

4. Take the 2-dimensional inverse Fourier transform of the Fourier plane to get the reconstructed image.

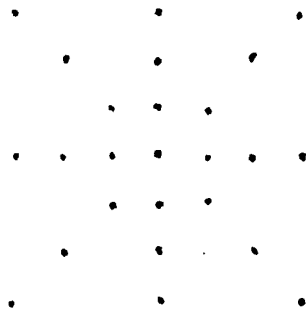


Figure 21 Concentric squares raster in the Fourier plane

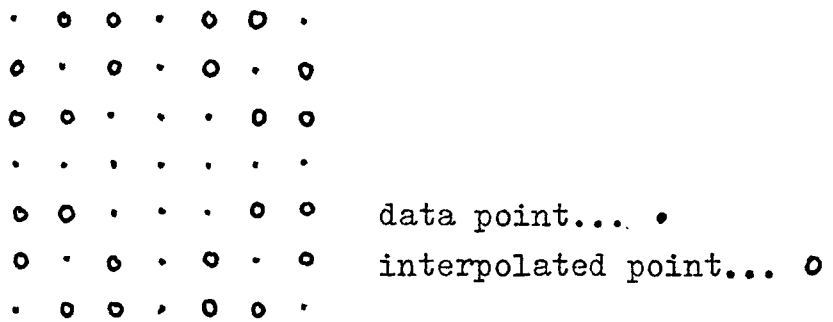


Figure 22 Cartesian raster

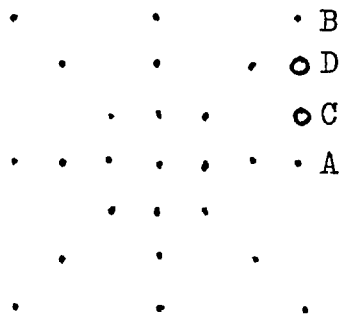


Figure 23 1-Dimensional interpolation from concentric squares raster to Cartesian raster

4.2 Application and Results

Following are some reconstructions of the 2-inch square specimen.

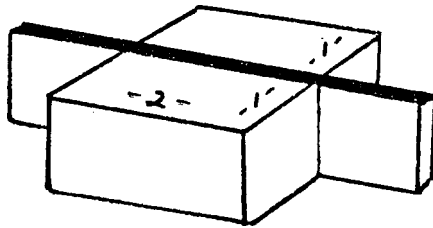


Figure 24a Orientation of output slice

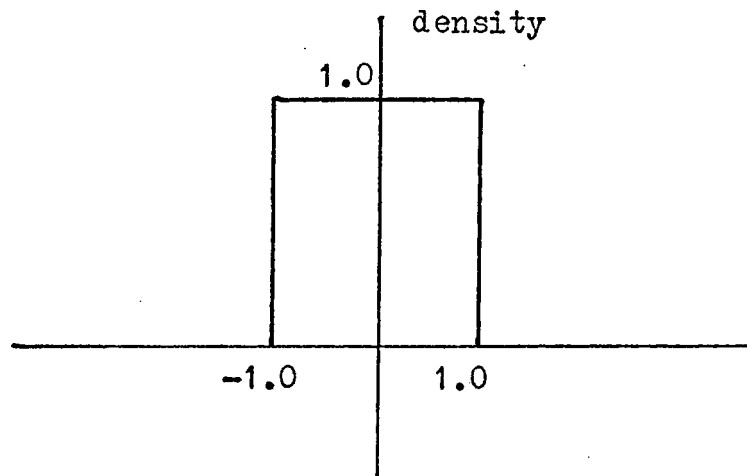


Figure 24b Ideal reconstruction



Figure 24c Actual reconstruction

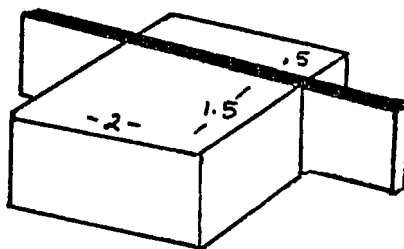


Figure 25a Orientation of output slice

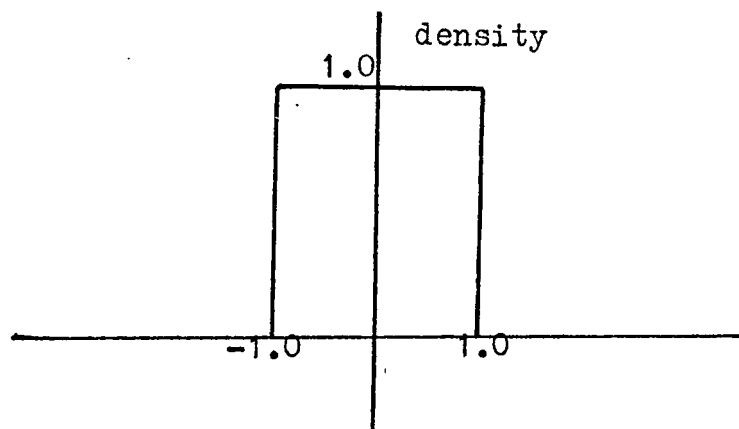


Figure 25b Ideal reconstruction



Figure 25c Actual reconstruction

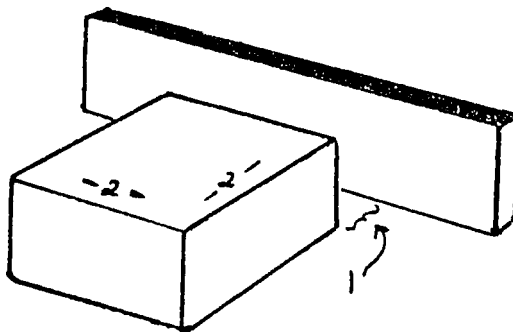


Figure 26a Orientation of output slice

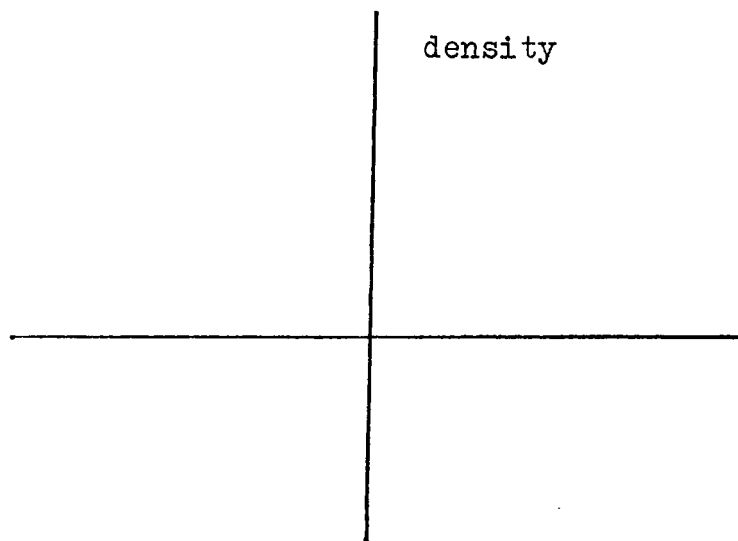


Figure 26b Ideal reconstruction



Figure 26c Actual reconstruction

4.3 Discussion

This program, too, runs quickly; making repeated use of the FFT. The results are relatively poor however. It appears the interpolation in only 1 dimension does not compensate in efficiency for the lack of input data available to 2-dimensional interpolation.

CHAPTER V

A FINAL WORD

5.1 Conclusions

There are two ways to evaluate the results of this study. First, the performance of each routine can be examined in a comparative sense. Is one routine better than another? Second, the results can be judged in an absolute mode. Are the methods cost effective? Do they measure up to expectations? Some of these points were discussed in previous chapters, but here we will take a broader look.

5.1.1 Comparison

The criteria by which we will compare the schemes should be stated at the outset. They are, run time, hardware requirements, and quality of output.

The 1-dimensional interpolation scheme runs a little faster than the 2-dimensional one, but both are considerably faster than the Hankel transform method. In fact if the Bessel functions must be generated for each Hankel transform, run times for that method can be prohibitive. By making a table of functions available to the program, this problem can be somewhat alleviated, however.

All three techniques require the input and output arrays be present in the computer at the same time. For the interpolation routines this means an array of 16 X 64 complex elements as well as one of 64 X 64 complex

elements must be on board. This reflects the fact that the input consists of 16 projections with 64 samples each, while the output consists of 64 rows and 64 columns from the Cartesian raster. Note here that complex numbers must be used since we are dealing with phasor quantities. The minimum requirements for the Hankel transform method are somewhat less - a 16 X 64 matrix on input as well as output. Remember here though that in addition, many memory locations must be reserved if a table of Bessel functions is to be input.

Apart from the size of computer memories, there is another hardware factor to be considered. The Hankel transform technique, in its interim steps, generates many large and small numbers. Depending on the machine, overflows and underflows can often result. This does not seem to be a problem with the interpolation routines.

The poorest reconstruction displays are produced by the 1-dimensional interpolation method. It apparently is severely handicapped by not being able to use all the data in the neighborhood of a point to be interpolated. At its best, the Hankel transform method can equal the 2-dimensional interpolation scheme in output quality, but this is very dependent on how well the Hankel integrals are calculated.

It is believed then, that the 2-dimensional interpolation method produces the best results and is the most cost effective.

5.1.2 Judgement

Now we ask the difficult question, "Are the findings satisfactory?" The reconstruction displays presented in this paper indeed reveal the general geometry of the simulated signals. Whether the accuracy and resolution is sufficient for practical purposes depends of course on the needs of the individual cases.

It is disturbing that the amount of memory required seems to rule out the use of mini-computers. What is worse, if it were desired to improve the calibre of results, even more data would have to be handled.

5.2 Suggestions

The problems and limitations encountered in this study do not lead into a dead end street however. Rays of hope do exist.

First, more sophisticated programming techniques might alleviate memory problems. Possibly the large arrays could be stored on some auxilliary disc while small parts of them would be shuffled in and out of the central processor.

Second, reconstruction algorithms could be amended to take advantage of any symmetries that might be known to exist in the object signal. Radial symmetry, for instance, can allow for dramatic reductions in memory usage and run time.

BIBLIOGRAPHY

1. J. Radon, On the Determination of Functions from their Integrals Along Certain Manifolds, Ber. Saechs. Akad. Wiss. Leipzig, Math. Physics Kl., vol. 69, pp. 262-277, 1917.
2. R.N. Bracewell, Strip Integration in Radioastronomy, Aust. J. Phys., vol. 9, pp. 198-217, 1956
3. H.J. Scudder, Introduction to Computer Aided Tomography, Proc. IEEE, vol. 66, pp. 628-637, 1978.
4. B.D. Cook and J.C. Berlinghieri, Calibration of Ultrasonic Fields from Acousto-Optic Data Using Fourier-transform Techniques: Theory, J. Acoust. Soc. Am., vol. 61, pp. 1477-1480, 1977.
5. B.D. Cook, Proposed Mapping of Ultrasonic Fields with Conventional Light Diffraction, J. Acoust. Soc. Am., vol. 65, pp. 682-684, 1975.
6. Image Processing for 2-D and 3-D Reconstruction from Projections: Theory and Practice in Medicine and the Physical Sciences, a digest of technical papers, 1975.
7. R.M. Mersereau, Recovering Multidimensional Signals from Their Projections, Computer Graphics and Image Processing, vol. 1, pp. 179-195, 1973.
8. R.M. Mersereau and A.V. Oppenheim, Digital Reconstruction of Multidimensional Signals from Their Projections, Proc. IEEE, vol. 62, pp. 1319-1338, 1974.
9. J.W. Cooley, P.A.W. Lewis, and P.D. Welch, Application of the Fast Fourier Transform to Computation of Fourier Integrals, IEEE Transactions on Audio and Electroacoustics, vol. AU - 15, pp. 79-85, 1967.

10. W.T. Cochran et al, What is the Fast Fourier Transform?, IEEE Transactions on Audio and Electroacoustics, vol. AU-15, pp. 45-55, 1967.
11. S. Bertram, On the Derivation of the Fast Fourier Transform, IEEE Transactions on Audio and Electroacoustics, vol. AU-18, pp. 55-58, 1970.
12. P.A. Stark, Introduction to Numerical Methods, The Macmillan Co., 1970.
13. T.R. McCalla, Introduction to Numerical Methods and FORTRAN Programming, John Wiley & Sons, 1967.
14. G. Arfken, Mathematical Methods for Physicists, Academic Press, 1970.

APPENDIX A

To show

$$\int_{-\pi}^{\pi} e^{j[\rho r \cos(\theta - \phi) - n\phi]} d\phi = 2\pi e^{-jn(\theta - \pi/2)} J_n(\rho r) \quad .$$

Let $\alpha = \phi - \theta + \pi/2$. This implies

$$\phi - \theta = \alpha - \pi/2,$$

$$\phi = \alpha + \theta - \pi/2,$$

and

$$d\phi = d\alpha \quad .$$

Since the cosine function is even, we have

$$\begin{aligned} \cos(\phi - \theta) &= \cos(\theta - \phi) \\ &= \cos(\alpha - \pi/2) \quad . \end{aligned}$$

Therefore

$$\int_{-\pi}^{\pi} e^{j[\rho r \cos(\theta - \phi) - n\phi]} = \int_{-\pi/2 - \theta}^{\pi/2 - \theta} e^{j[\rho r \cos(\alpha - \pi/2) - n(\alpha + \theta - \pi/2)]} d\alpha \quad (30)$$

$$= e^{-jn(\theta - \pi/2)} \int_{-\pi/2 - \theta}^{\pi/2 - \theta} e^{j[\rho r \sin \alpha - n\alpha]} d\alpha \quad (31)$$

where we have made use of the identity

$$\cos(\gamma - \pi/2) = \sin \gamma \quad .$$

By using basic trigonometric identities, it can be easily shown that the integrand of equation 31 is periodic with period 2π . Consequently the value of the integral is the same over any range of 2π . Therefore changing the limits in that equation, we get

$$\int_{-\pi}^{\pi} e^{j[\rho r \cos(\theta-\phi) - n\phi]} d\phi = e^{-jn(\theta-\pi/2)} \int_{-\pi}^{\pi} e^{j[\rho r \sin \alpha - n\alpha]} d\alpha \quad (32)$$

Expansion of the exponential function reveals

$$\int_{-\pi}^{\pi} e^{j[\rho r \cos(\theta-\phi) - n\phi]} d\phi = e^{-jn(\theta-\pi/2)} \left[\int_{-\pi}^{\pi} \cos(\rho r \sin \alpha - n\alpha) d\alpha + j \int_{-\pi}^{\pi} \sin(\rho r \sin \alpha - n\alpha) d\alpha \right] \quad (33)$$

The integrand of the first term is an even function; the integrand of the second, odd. This implies then that

$$\int_{-\pi}^{\pi} e^{j[\rho r \cos(\theta-\phi) - n\phi]} d\phi = 2e^{-jn(\theta-\pi/2)} \int_0^{\pi} \cos(\rho r \sin \alpha - n\alpha) d\alpha \quad (34)$$

$$= 2\pi e^{-jn(\theta-\pi/2)} \int_0^{\pi} \frac{1}{\pi} \cos(\rho r \sin \alpha - n\alpha) d\alpha \quad (35)$$

But the integral in equation 35 is one of the well known representations of the Bessel function. Thus

$$\int_{-\pi}^{\pi} e^{j[\rho r \cos(\theta-\phi) - n\phi]} d\phi = 2\pi e^{-jn(\theta-\pi/2)} J_n(\rho r) \quad (36)$$